CHAPTER 6

DESIGN AND SIMULATION STUDIES OF SECOND HARMONIC GYRO-TWT WITH 3-FOLD HELICALLY CORRUGATED WAVEGUIDE

6.1. Introduction

6.2. Helically Corrugated Waveguide

6.3. Dispersion Characteristics of Helically Corrugated Waveguide

6.3.1. Analytical Method

6.3.2. Numerical Method

6.4. Design of Circular TE_{11} Mode Input Coupler

6.5. PIC Simulation of Gyro-TWT with Helically Corrugated Waveguide

6.5.1. Modeling of the Interaction Circuit

6.5.2. Simulation Results and Parametric Study

6.5.3. Double Disk Output Window

6.6. Conclusion

*Part of this work has been submitted as:

Akash and M. Thottappan, "Design and Simulation Studies of Second Harmonic W-band Gyrotron Travelling Wave Amplifier with helically corrugated interaction structure", *XXXXXXXXXXXXXXX*.

6.1. Introduction

The gyro-TWT with helically corrugated waveguides has been jointly studied at the Institute of Applied Physics (IAP), Russia and University of Strathclyde (UOS), U.K. [Denisov *et al.* (1998), Bratman *et al.* (2000), Cross *et al.* (2007), Samsonov *et al.* (2014), He *et al.* (2017)]. The helically corrugated waveguide has been used as an RF interaction system for gyro-TWT [Bratman *et al.* (2000)] and gyro-BWO [He *et al.* (2013)] and also in high power pulse compressor, where it serves as a dispersive medium [Burt *et al.* (2005)]. The main objective of the use of helical waveguide is the radical variation of the smooth waveguide dispersion near the area of very low axial wavenumber. The helical disturbance inside smooth waveguide can provide selective coupling between a close to cut-off mode and a far cut-off mode. By this coupling, an Eigen wave with a finite and almost constant group velocity in the region of close to zero ax*i*al wave number is created. The resultant eigenwave provides the favorable dispersion for gyro-TWT with broadband characteristic and weak sensitivity to axial beam velocity spread [Denisov *et al.* (1998)]. To achieve the desired waveguide dispersion, the helically corrugated waveguide with mean radius of 'r_0' should couple the two-partial wave; one partial wave (mode-1) with close to cut-off axial wavenumber, $k_{z,1} << k$, where, $k = r_0$ /c, the second partial wave (mode-2), with large axial wavenumber, $k_{z2} \sim k$. Mode-1 is co-rotating with the helical corrugation (both are in same direction) but the mode is not perturbed by the corrugation. Mode 2 is counter rotating with the helical corrugation (both are in opposite direction) but the mode is strongly perturbed by the corrugation and allowed the dispersion to change radically. The group velocity of the resultant Eigen wave can be changed and adjust close to the beam axial velocity in the region of zero axial wave number.

With the help of cyclotron resonance condition for helical electron beam that interacting with a waveguide mode of operating frequency 'ω' and axial wave number k_z, the sensitivity of efficiency and bandwidth to axial velocity spread in gyro-TWT can be explained as follows,

$$\omega - k_z \upsilon_z = \frac{s\Omega_0}{\gamma} \tag{6.1}$$

where, $\Omega_0 = eB/m_{e0}$ is the non-relativistic electron cyclotron frequency; 's' is the harmonic number; v_z and γ are the axial velocity of electrons and Lorentz factor, respectively. This phase-matching condition states that as gyro-TWT is operated at large k_z, a large value of axial velocity spread can vary the Doppler shift and disturbed this phase-matching beam beam-wave interaction. To overcome this disturbance, the effect of a small periodic helical corrugation on inner surface of circular waveguide is considered. The two modes are resonantly coupled such that one of the modes is having close to cut-off axial wave number and other mode is a propagating one with large axial wave number.

In this chapter, 3D electrodynamic numerical model of a W-band second harmonic gyro-TWT amplifier with a 3-folded helically corrugated interaction waveguide has been benchmarked with an experiment performed by Prof. He and his group [He *et al.* (2017)] for high data rate ground-based telecommunication network and cloud profiling radar applications. He *et al.* has tested the gyro-TWT experimentally and observed a saturated RF power and gain of ~3.4 kW and ~38 dB at 9 GHz, respectively. This amplifier offered 3-dB bandwidth of ~5.5 GHz (restricted by the bandwidth of input source i.e., 91-96.5 GHz).

6.2. Helically Corrugated Waveguide

In a cylindrical coordinate system, the helically corrugated waveguide profile is represented by [Denisov *et al.* (1998)],

$$r(\varphi, z) = r_0 + r_1 \cos(m_B \varphi + k_B z) \tag{6.2}$$

where, r_0 and r_1 are the mean radius of waveguide and corrugation amplitude respectively. m_B and k_B are the azimuthal and axial wavenumber of the Bragg periodicity vector, where, $k_B = 2\pi / d$, and d is the corrugation period of the waveguide. A schematic of such a 3-fold corrugated waveguide is shown in Figure 6.1 and the dimensions of 3-fold helically corrugated waveguide are listed in Table 6.1. The two circularly polarized modes are resonantly coupled once the axial and azimuthal wavenumbers of these modes fulfill the Bragg conditions which are given by,

$$m_B = m_1 - m_2; \qquad k_B = k_{z1} - k_{z2} \tag{6.3}$$

where, m_1 and m_2 are the azimuthal indices and k_{z1} and k_{z2} are the axial wavenumbers of the two modes. The helical corrugations in the waveguide result in the coupling of the two modes and generate Eigen waves with most favorable dispersion characteristics for gyro-TWT over the large frequency band. The 3-fold helically corrugated waveguide has been also used in the compression experiments with a right-handed helical corrugation, where m_B = −3, the corrugated structure resonantly coupled a forward propagating left-circularly polarized *TE*-$_{1,1}$ mode (m_1 = -1) and a near cut-off right-circularly polarized $TE_{2,1}$ mode (m_2 = 2) in the lowest frequency band [Burt *et al.* (2004), (2005)].

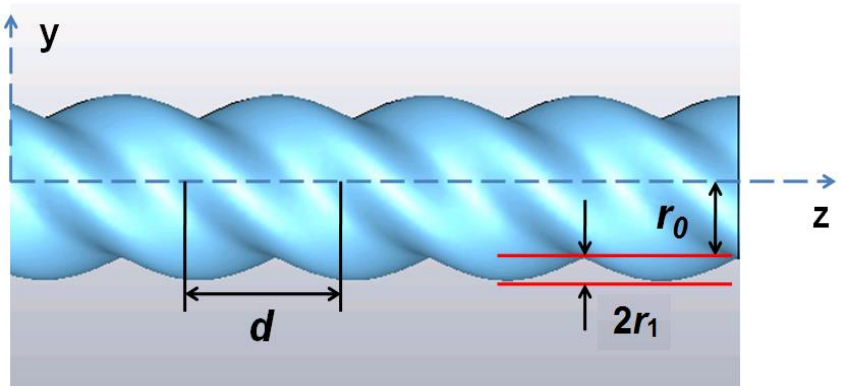

Figure 6.1: Schematic of 3-folded helically corrugated waveguide.

Table 6.1: Design Parameters of 3-Folded Helically corrugated Waveguide

Waveguide parameter	Value
r_0	1.47 mm
r_1	0.23 mm
d	3.2 mm
m_B	-3
$k_B = 2\pi / d = 2\pi /3.2$	1.963 mm^{-1}

6.3. Dispersion Characteristics of Helically Corrugated Waveguide

6.3.1. Analytical Method

The 3-folded helically corrugated waveguide couples the corotating TE_{21} mode with the counter rotating circularly polarized TE_{11} mode. The coupling of these two modes generates an operating Eigen wave, as shown in Figure 6.2. The dispersion of the resultant Eigen wave can be computed with the help of the coupled mode theory [Cooke *et al.* (1998), Zhang *et al.* (2015), Katsenelenbaum *et al.* (1999)]. The coupled mode theory states that for a small corrugation amplitude ($r_1 << r_0$), the resultant Eigen wave of helically corrugated waveguide by the coupling of two modes can be found using the following Eigen mode dispersion equation.

$$f_{m_1}^2(k_z) \,.\, f_{m_2}^2(k_z) = 4\kappa^2 k_0^4 \tag{6.4}$$

where, κ is the coupling coefficient which represents the coupling strength between the two modes. The coupling coefficient can be given by,

$$\kappa = \frac{r_1}{2r_0^3 k_0^2} \frac{\chi_1^2 \chi_2^2 - m_1 m_2 r_0^2 (k_0^2 + k_{z1} k_{z2})}{\sqrt{(\chi_1^2 - m_1^2)(\chi_2^2 - m_2^2)}} \tag{6.5}$$

κ is normalized with wavevector k_0 *i.e.* $k_0 = \sqrt{k_{z1}^2 + k_{\perp 1}^2}$. χ_1 and χ_2 are the Eigen value of the mode 1 and mode 2, respectively. The function $f_{m1}(k_z)$ and $f_{m2}(k_z)$ are the dispersion relations of modes to be coupled, which is a function of the axial wave number, k_z. The dispersion relation $f_{m1}(k_z)$ of the mode 1 can be written as,

$$f_{m_1}^2(k_z) = (k^2 - k_z^2 - k_{\perp 1}^2) \tag{6.6}$$

where, $k_{\perp 1}$ is the transverse wavenumber of mode 1 (TE_{21} mode).

The mode-2 is the negative spatial harmonic of TE_{11} mode therefore, the dispersion curve of mode-2 is sifted to the left by k_B and this can be written as,

$$f_{m_2}^2(k_z) = (k^2 - (k_z - k_B)^2 - k_{\perp 2}^2) \tag{6.7}$$

where, $k_B = 2\pi / d$ and $k_{\perp 2}$ is the transverse wavenumber of mode 2 (TE_{11} mode). The dispersion relation expressed in equation (6.3) is fourth order linear equation and its solution leads to four Eigen values. Out of four Eigen values, only two Eigen waves have practical or physical importance and can be called as upper operating wave W_1 and lower operating wave W_2. As the coupling coefficient, $\kappa = 0$, i.e., there is no coupling between the modes, the resulting Eigen function will degenerate into two separate dispersion function that is, $f_{m_1}^2(k_z) = 0$ and $f_{m_2}^2(k_z) = 0$. The W_1 and W_2 will also degenerate into previous uncoupled partial waves. The dispersion equation (6.3) is expanded, which results in a fourth order polynomial given by,

$$k^4 - k^2\left[(k_z + k_B) + k_{\perp 1}^2 + k_{\perp 2}^2 + k_z^2\right] + \left(k_z^2 + k_{\perp 1}^2\right)\left[k_{\perp 2}^2 + (k_z + k_B)^2 - \kappa^2\right] = 0 \tag{6.8}$$

This expanded equation is solved numerically to find the roots of the coupling coefficient (κ). The design parameters of the present 3-folded helically corrugated waveguide including the average radius, corrugation depth and period of the helical waveguide are utilized in the computation. In the present analysis, mode 1 is corresponding to $TE_{2,1}$ mode and mode 2 is corresponding to $TE_{1,1}$ mode. The Bessel's function roots have been computed for both $TE_{1,1}$ and $TE_{2,1}$ modes. The cut-off wave number for mode 1, $TE_{2,1}$ mode, is calculated as,

$$k_{\perp 1} = \frac{3.054}{1.47} = 2.08\, mm^{-1}$$

Similarly, the cut-off wave number for mode 2, TE_{11} mode, is calculated as,

$$k_{\perp 2} = \frac{1.841}{1.47} = 1.25\ mm^{-1}$$

The axial Bragg periodicity vector (k_B) is calculated by using the value of the longitudinal period of helical corrugation, d = 3.2 mm,

$$k_B = \frac{2\pi}{3.2} = 1.96\ mm^{-1}$$

The coupling coefficient, κ is calculated from equation (6.4),

$$\kappa = \frac{r_1}{2r_0^3 k_0^2} \frac{\chi_1^2 \chi_2^2 - m_1 m_2 r_0^2 (k_0^2 + k_{z1} k_{z2})}{\sqrt{(\chi_1^2 - m_1^2)(\chi_2^2 - m_2^2)}}$$

The corrugation amplitude, r_1 is 0.23 mm, and k_{z1} and k_{z2} are calculated as follows:

$$k^2 = k_{\perp 1}^2 + k_z^2 \tag{6.10}$$

$$k^2 = k_{\perp 2}^2 + \left(k + k_B\right)^2 \tag{6.11}$$

$$k_{z1} = -\left(\frac{k_{\perp 1}^2 - k_{\perp 1}^2 - k_B^2}{2k_B}\right) \tag{6.12}$$

$$k_{z2} = k_B - k_{z1} \tag{6.13}$$

where, k_0 is the wavevector of exact Bragg resonance and is the intersection point of the coupled modes. It is calculated from $k_0 = \sqrt{k_{z1}^2 + k_{\perp 1}^2}$.

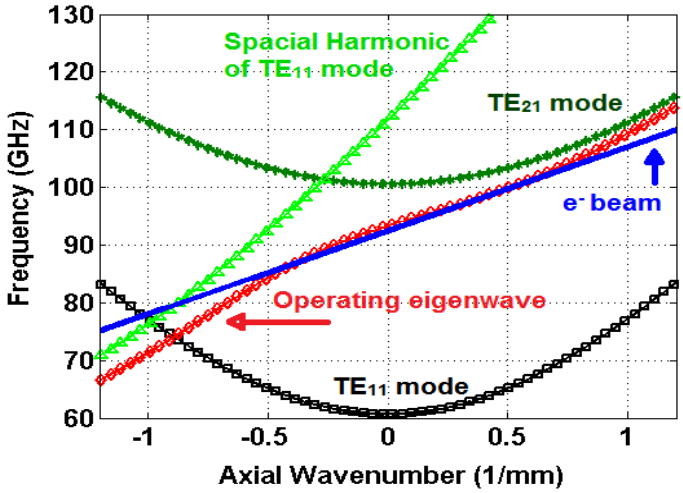

Figure 6.2: Dispersion diagram of 3-folded helically corrugated waveguide using coupled mode theory (V_0 = 55kV, I_0 = 1.5 A, B_0 = 1.82 T).

6.3.2. Numerical Method

The numerical dispersion calculation of helically corrugated waveguide has been done by using "CST Microwave Studio". The electromagnetic behavior of the closed resonant structures is analyzed using the Eigenmode Solver. In the present study, a single period length 3-folded helically corrugated waveguide structure is modeled to compute the Eigen-frequencies and field distribution of the modes. A single period of the 3-folded helically corrugated waveguide can be modeled in CST by two methods. The first method is by using the visual basic application (VBA) macro program. In this method, first an outline of the front face of the 3-folded helically corrugated waveguide is generated as shown [Figure 6.3(a)], then using the extrude option of graphical user interface (GUI) feature in CST, the curve outline is extruded to one period length (d) as shown in Figure 6.3(b). This extruded shape is twisted by 120^0. The angle of twist is calculated as 360° divided by the number of folds. For the present case the angle of twist is 120°, which is inputted as a positive number in "CST Microwave Studio" to give the twist in the clockwise direction as a representative for the 3-fold helically corrugated waveguide [Figure 6.3(c)]. Another method of modeling 3-folded helically corrugated waveguide is by using the analytical face in modeling section of "CST Microwave Studio". Here, the surface of the helically corrugated waveguide [Figure 6.4(a)] is created using the analytical equation (6.3). This thin surface is converted into the solid waveguide by covering the input and output cross-section of the helical surface as shown in Figure 6.4(b). The CST Eigen mode solver is used to calculate the Eigen frequencies within the frequency range of 60GHz to 120GHz. The boundary phase angle (θ) is varied from -180° to 180° degrees at 5° intervals and for each Eigen frequency the corresponding axial wavenumber is calculated using the relation, $k_z = \theta /d$, where, θ is in radians and d is the corrugation period. The Eigen mode simulation

has been carried out for 10 odd modes. The results from the CST Eigen mode solver are plotted to show the Eigen mode dispersion [Figure 6.5], in which the dashed line shows the operating Eigen mode dispersion corresponding the Eigen frequency of each mode. The comparison of dispersions using both the coupled mode theory and numerical simulation of CST is shown in Figure 6.6.

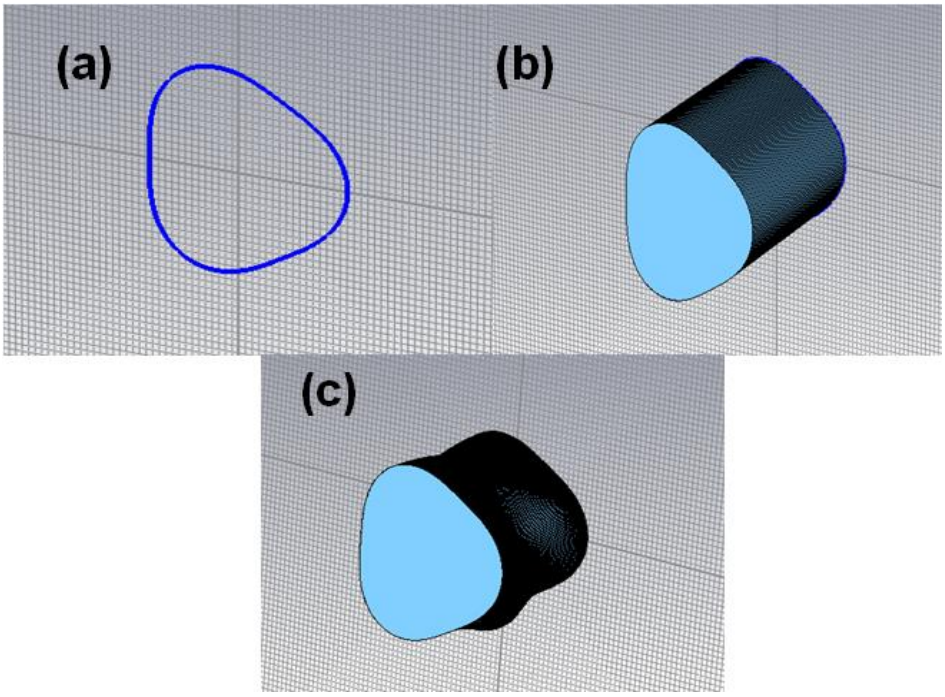

Figure 6.3: Modeling of 3-folded helically corrugated waveguide using VBA macro program in CST (r_0 = 1.47 mm, r_1 = 0.23 mm, d = 3.2 mm) (a) outline of the 3-fold face (b) extruded model (c) 120^0 twisted model.

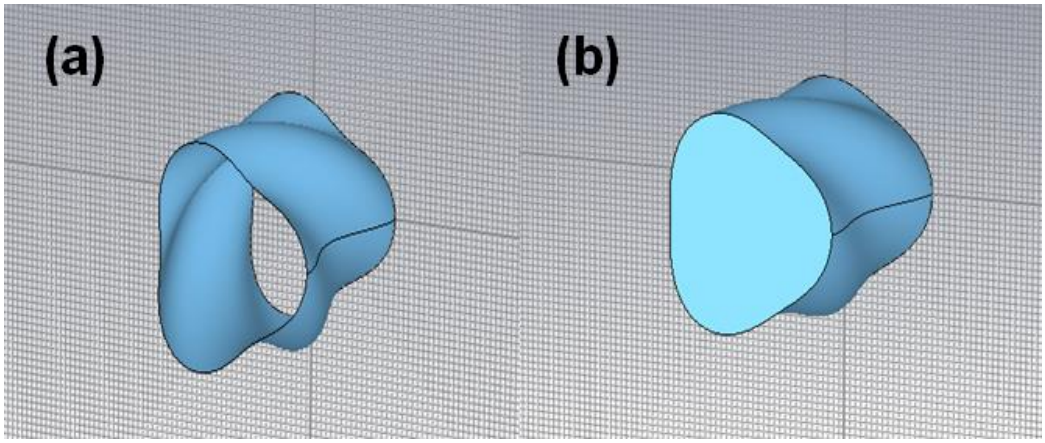

Figure 6.4: Modeling of 3-folded helically corrugated waveguide using analytical modeling in CST (r_0 = 1.47 mm, r_1 = 0.23 mm, d = 3.2 mm) (a) 2D thin surface of 3 folded corrugated waveguide (b) 3D model after covering up the faces.

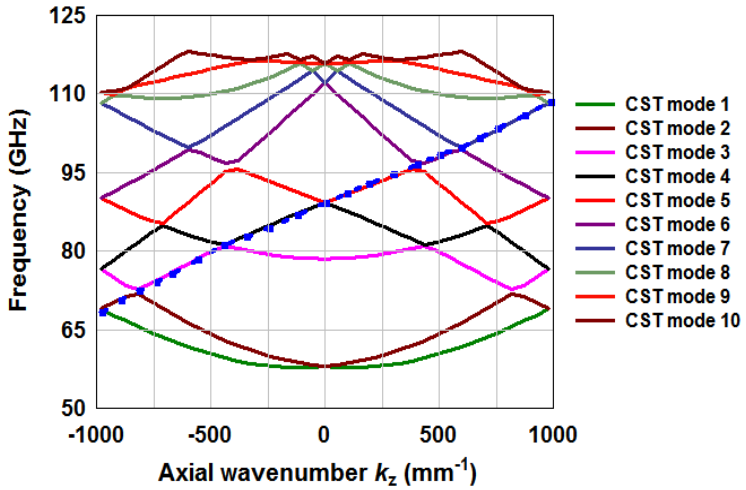

Figure 6.5: Dispersion diagram using CST Microwave Studio with the dotted line indicating the operating eigenwave.

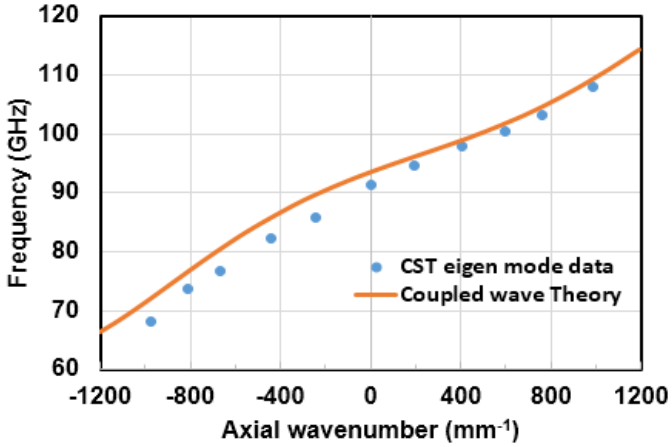

Figure 6.6: Comparison of calculated dispersion using coupled mode theory and 'CST Microwave Studio'.

6.4. Design of Circular TE_{11} Mode Input Coupler

To feed the 3-folded helically corrugated waveguide gyro-TWT amplifier, an input coupler is needed, which can convert the fundamental waveguide mode into the left hand circular polarized TE_{11} mode. Figure 6.5 shows the proposed circular polarization TE_{11} mode coupler. The present coupler consists of two stages of mode processes. The first stage is the side wall coupling section [Zhang *et al.* (2005)], where an input wave from the fundamental rectangular waveguide mode at port 1 is coupled to the circular waveguide through the side wall coupling [Figure 6.7(a)]. The fundamental

TE_{10} mode from the rectangular waveguide is injected into a circular waveguide through the side wall coupling to generate a TE_{11} mode with linear polarization. The next stage is the polarization-converting stage [Figure 6.7(b)], where this linearly polarized TE_{11} wave propagates into a sinusoidal corrugated rectangular waveguide section to generate a TE_{11} wave at port 2 with left circular polarization [Robertson *et al.* (2013)]. The side-wall input coupling stage of the input coupler consist of a standard rectangular waveguide (WR-10) that is attached at the right angle by the sidewall of the circular waveguide. There is one cut-off waveguide attached left to the circular waveguide. The main purpose of connecting the cut-off waveguide is to cause the RF signal propagates in the forward direction only. The cut-off waveguide is also served as the electron beam tunnel for the gyro-TWT operation. Therefore, the inner radius of the cut-off waveguide should be small enough to effectively suppress the parasitic modes and as large enough to pass the beam into the RF interaction circuit. The CST model of the linearly polarized TE_{11} mode section is shown in Figure 6.7(a). The circular waveguide radius is set equal to the mean radius of helically corrugated waveguide, while the radius of the cut-off waveguide is optimized between $0.7r_w$ to $0.8r_w$ in order to minimize the backward propagation of the wave. The second stage of the input coupler is the stage of polarization transition stage. in which the linearly polarized TE_{11} mode / wave is entered at the input and converted into the circular polarized TE_{11} mode at the output port through the sinusoidally corrugated rectangular waveguide. The optimized dimensions of the corrugated rectangular waveguide are a = 2.7 mm, b = 2. mm, L= 11.5mm, n = 12, and q = 0.2 mm, where, a and b are broad and narrow side dimensions of the rectangular waveguide, L is length of the rectangular waveguide, n is the total number of corrugation and q is the corrugation amplitude, respectively.

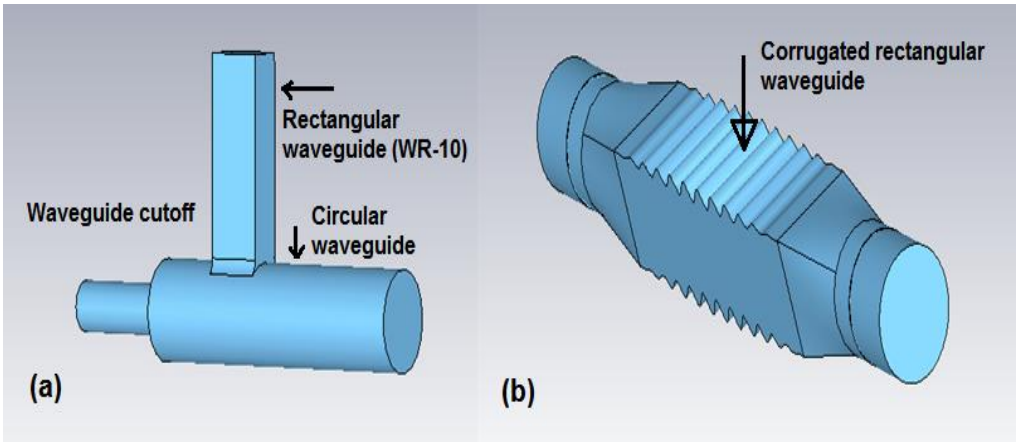

Figure 6.7: (a) Side wall coupling stage to convert the fundamental rectangular TE_{10} mode into linearly polarized circular waveguide TE_{11} mode and (b) circular TE_{11} mode polarizer with corrugated rectangular waveguide.

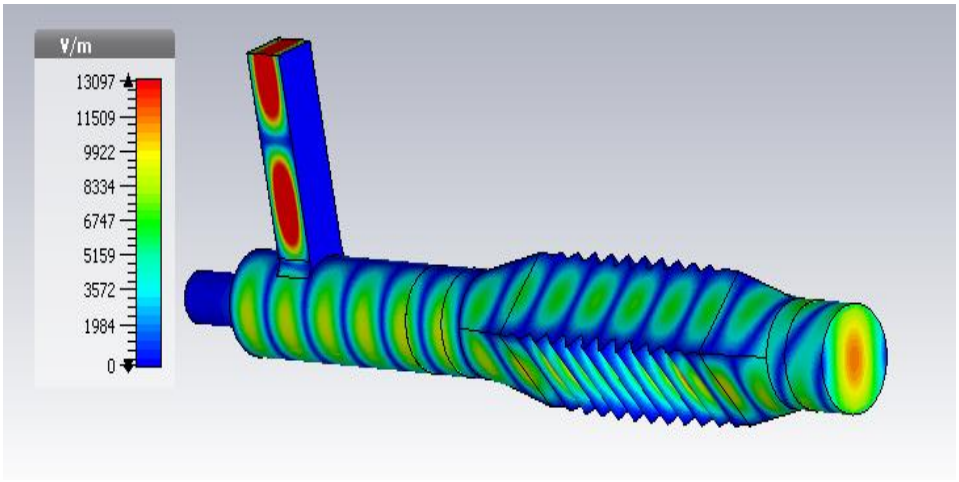

Figure 6.8: Distribution of electric field at each stage of the input coupler.

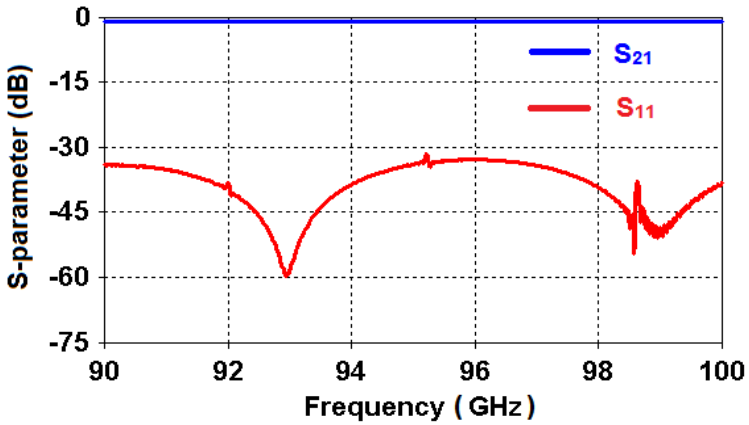

Figure 6.9: S-parameter results of circular TE_{11} mode input coupler.

Now, the complete CST model of the input coupler is taken into consideration for the cold simulation and development of electric field within the coupler. The fundamental TE_{10} mode is fed into the rectangular waveguide [Figure 6.8], which is converted into a linearly polarized TE_{11} mode at the end of circular waveguide of sidewall coupler stage. This circular TE_{11} mode is acted as the input to the rectangular corrugated stage. The polarized transitional stage is tilted 45^0 with respect to the polarization of linearly polarized TE_{11} mode at the end of the sidewall coupling stage. After propagating through the circular to rectangular convertor, the E-field is distributed into TE_{01} and TE_{10} modes along the sides of corrugated waveguide. The corrugation alters E-field distribution of one of the modes and make it hybrid in nature, whereas the field of the other mode remains unaltered. The two waves get 90° phase difference as they propagate through the corrugated rectangular section, after that waves entered into the circular waveguide section where both the out of phase waves are added and form a circularly polarized. The E-field distribution within the input coupler is shown by the contour plot [Figure 6.8]. The S-parameters results of the present input coupler are shown in Figure 6.9 that shows a good performance with transmission coefficient (S_{21}) of ~0.5 dB and reflections less than 30 dB over the operating frequency band.

6.5. PIC Simulation of gyro-TWT with Helically Corrugated Waveguide

6.5.1. Modeling of the Interaction Circuit

The present W-band gyro-TWT amplifier operating at second harmonic and employing 3-folded helically corrugated interaction structure is modeled and simulated using CST-PIC. This numerical model has been benchmarked to a W-band gyro-TWT experiment performed by Prof. He and his group [He *et al.* (2017)]. This experimentally tested gyro-TWT produced a maximum of 3.4 kW RF power at the operating frequency

of 94 GHz. The calculated maximum gain was 38 dB and ~5.5 GHz 3-dB bandwidth (limited by the power and bandwidth of input source i.e., 0.52 W for 91-96.5 GHz frequency range). The present electrodynamic model consists of a linear TE_{11} to circular TE_{11} mode input coupler, sections of up- and down- taper of length of four periods to convert the circular to helical waveguide and vice versa, a regular corrugation section of 16 periods and a tapered section (cone) with 9 periods of length. All these sections are first modeled with vacuum [Figure 6.10(a)] and then cut from a rectangular cuboid of copper metal [Figure 6.10(b)]. The structural and electrical parameters of the amplifier are given in Table 6.2. In the practical design of gyro-TWT, the electron beam is formed in the electron gun and deposited on the inner surface of the collector by passing through the interaction region. Since, the electron gun and collector both are electrically huge component and including them into the numerical model requires a very high meshing and large computation time and sometime reaches beyond the simulation tool capabilities, therefore, it is required to simulate each component independently.

Table 6.2: Design and Electrical Parameters of Gyro-TWT.

Parameter	**Value**
Mean Radius, r_0	1.47 mm
Corrugation Amplitude, r_1	0.23 mm
Corrugation Period, d	3.2 mm
Number of Fold, m_B	-3
Brag Periodicity Vector $k_B = 2\pi / d = 2\pi / 3.2$	1.963 mm^{-1}
Regular Corrugation Length	16 Period
Up Taper Length	4 Period
Down Taper Length	4 Period
Cone Length	9 Period
Voltage, V_0	55 kV
Current, I_0	1.5 A
Operating Frequency, f	95 GHz
Pitch Factor	1.2
Magnetic Field, B_0	1.82

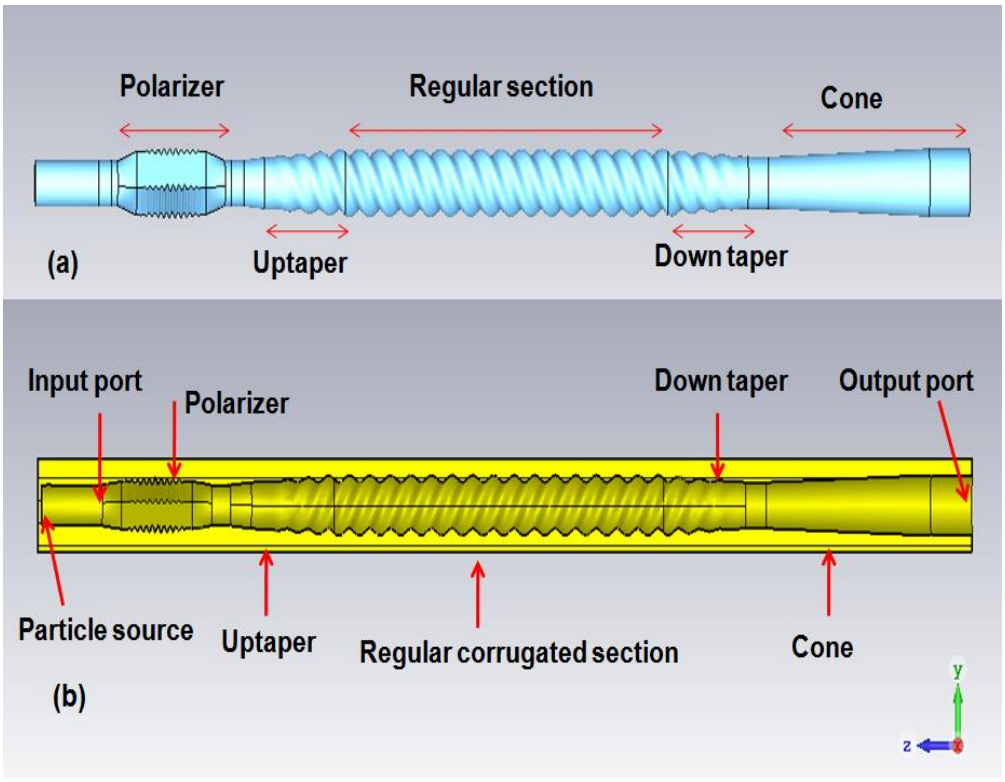

Figure 6.10: The 3D electrodynamic model for the PIC simulation of gyro-TWT with 3-fold helically corrugated structure (a) modeled in vacuum (b) after cutting the vacuum model from a rectangular cube.

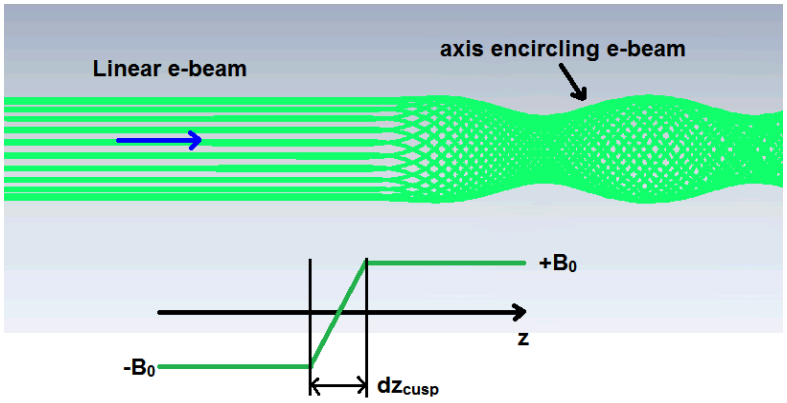

Figure 6.11: An axis encircling beam from a particle source of hollow ring with artificial magnetic cusp.

However, for the PIC simulation of RF interaction circuit using CST, a particle source is created on a hollow metallic ring, that initially produced the rectilinear electron beam [Figure 6.11]. After a short distance, an artificial magnetic cusp is placed to give the transverse momentum to similar to the axis encircling electron beam. The width of the artificial cusp (dz_{cusp}) is used to define the transverse velocity spread while the mean

ring radius defines the average velocity ratio. By this modeling of particle source, one can produce the beam characteristic very close to the beam generated by an axis encircling gun.

6.5.2. Simulation Results and Parametric Study

For the simulation of numerical model of helically corrugated waveguide gyro-TWT, the electrical parameters are borrowed from the experimentally performed gyro-TWT [He *et al.* (2017)]. A DC electron beam (55 kV, 1.5 A) with unity velocity ratio (α) and 10% spread in α is emitted from particle source of hollow ring with an artificial cusp (magnetic field reversal). In the PIC simulation, the RF input with a linear polarized TE_{11} mode is applied at the input of the rectangular corrugated polarizer, which is converted into the left-handed circular polarized TE_{11} wave. Inside the waveguide, this wave is counter-rotating with the helical corrugation and is strongly coupled with the co-rotating TE_{21} mode of simple smooth circular waveguide and results an operating Eigen wave of the helically corrugated waveguide. This resulting operating Eigen wave is interacting with the axis encircling (cusp gun) electron beam. During the interaction process, the electron beam transfers its kinetic energy to the operating Eigen wave, hence the operating Eigen wave is converted into the circular waveguide TE_{11} mode as it passes through the down taper (helical to circular waveguide converter). The amplified RF beam is collected at the output port after passing through a slightly tapered waveguide. The circular TE_{11} mode is azimuthally asymmetric, which is divided into the linearly polarized modes (mode1 and mode 2). Therefore, the output will be the sum of the power at mode 1 and mode 2 and can be calculated as (2*(E-filed amplitude) ^2 / 2). The temporal electric field growth and output power plots are shown in Figures 6.12(a) and 6.12(b), respectively. The PIC simulation predicted an RF output

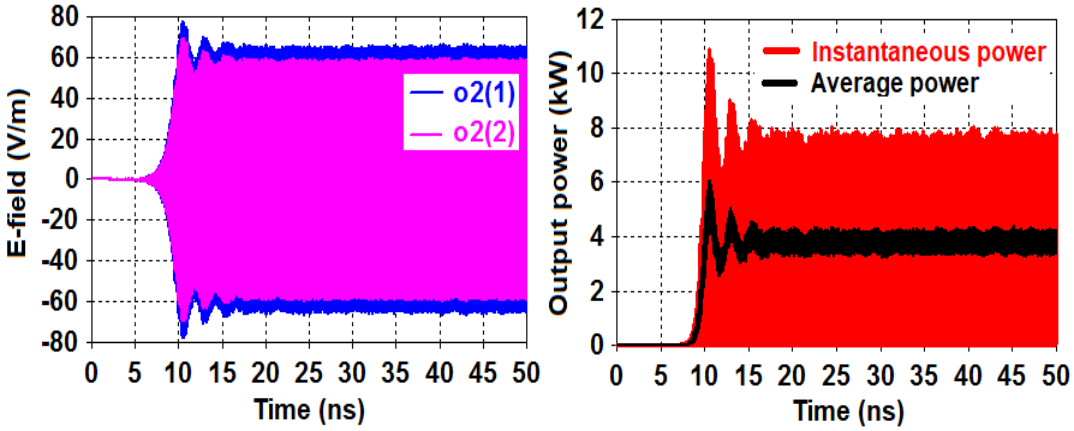

Figure 6.12: Temporal growth of amplified (a) E-field and (b) power at the output port (Pin = 0.52W).

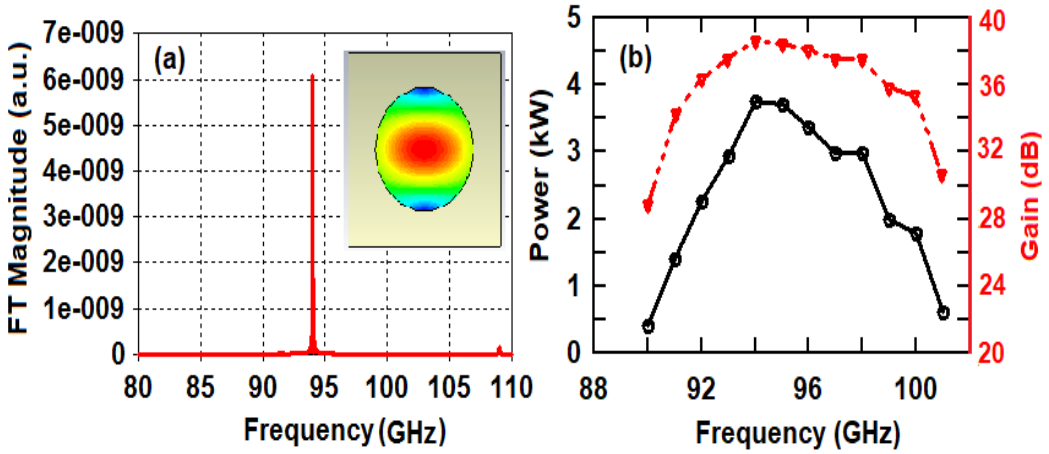

Figure 6.13: (a) FFT plot of the amplified signal and (b) power and gain plot as function of frequency.

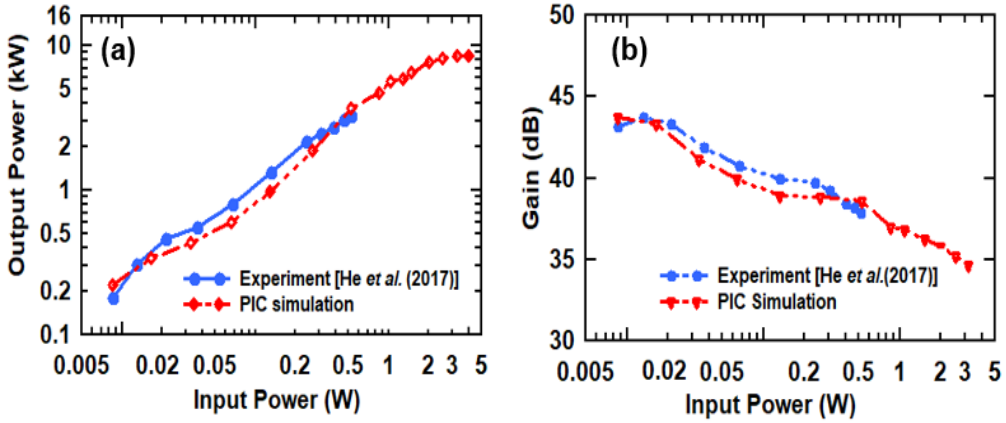

Figure 6.14: Comparison of (a) transfer characteristic and (b) gain Vs input power between experiment and PIC simulation.

power of ~3.75 kW in TE_{11} mode at 94 GHz for an axis encircling beam with 10% spread in α. The Fast Fourier transform of the RF output signal is obtained using the post processing feature of CST, which peaks at 94GHz [Figure 6.13(a)]. The RF power is calculated for different frequencies ranging from 90-101GHz by keeping other parameters as constant [Figure 6.13(b)]. The PIC simulation results are observed to be in close agreement with the experimental results [He *et al.* (2017)] at 94 GHz. The 3-dB bandwidth of the present gyro-TWT has been predicted as ~8 GHz by the simulation. Figure 6.14(a) shows the comparison of the present simulated RF output power with the experimentally tested one for different RF input power at 94 GHz. Due to the limitation of input source power up to 0.52 W, the experimental results were unable to predict the saturated output. However, the PIC simulation results predicted that the output power is increased as the input power is increased and the saturation in power (~9.2 kW output power) is observed for the input power of ~3W. Similarly, Figure 6.14(b) shows the comparison between the experimentally measured gain and simulated gain for different input power at 94 GHz. It is observed from the figure that the gain is decreased gradually as the RF input power is increased. However, a close agreement between the experimental and simulated gains is observed, i.e., ~38 dB and ~38.5dB, respectively, for an RF input power of 0.52W.

6.5.3. Double Disk Output Window

A TE_{11} mode double disk window is used to extract the output power. The Boron Nitride (BN) has been chosen as the disk material. As compared with the sapphire window, Boron Nitride (BN) window offers the low insertion loss and high thermal conductivity (1.38 times higher), and also has higher bandwidth with better edge cooling [Kesari *et al.* (2013)]. The window disk thickness (t) should be equal to the integer multiple of half wavelengths ($t = n\lambda_g / 2$, n = integer) in disk material

medium. The distance or gap (d) between the two disks should satisfy the following condition to have the low reflection at the window,

$$\beta_z \, d = (n + \tfrac{1}{2})\, \pi$$

where, β_z is the axial wavenumber between the disk or empty waveguide and n is an integer. In the present case, the window disk thickness and gap between the disks are calculated as 0.735 mm and 1.02 mm, respectively. The cold simulation results of the double disk BN window along with CST model and the contour of TE_{11} mode is shown in Figure 6.15. The simulation results predicted that the transmission coefficient is lower than −20.8dB and reflection coefficient is better than −0.04 dB for the operating frequency bandwidth of 10 GHz (90-100 GHz).

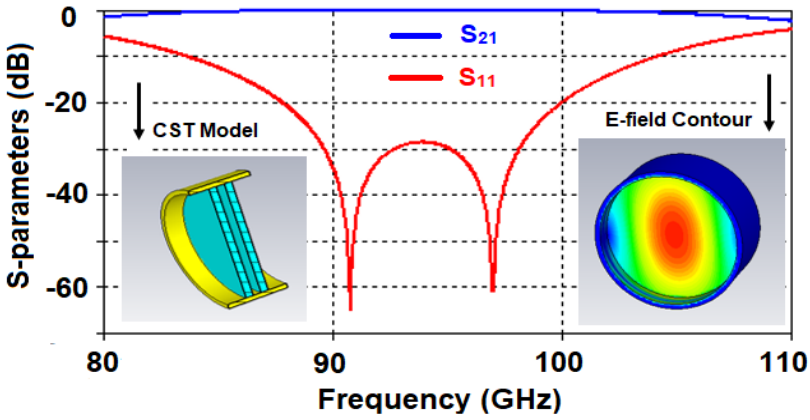

Figure 6.15: The cold simulation result of double disk BN window along with CST model and E-field contour (inset).

6.6. Conclusion

A 3-folded helically corrugated waveguide for a W-band second harmonic gyro-TWT has been modelled and benchmarked with an experimentally tested amplifier [He *et al.* (2017)]. The Eigen mode dispersion of the 3-folded helically corrugated waveguide has been calculated using coupled mode theory and compared with its numerical computation using "CST Microwave Studio". The PIC simulation has been carried out by modeling an electrodynamic model close to the experimental one. The

simulation of the present gyro-TWT predicted an RF output power of ~3.75 kW at 94 GHz, 38.5 dB gain and 3-dB bandwidth of ~8 GHz. A double disk window has been designed and simulated to extract the output power with minimum reflections. The window was found to have less that -20dB reflection over the frequency range of 90-100 GHz. The present PIC simulation results of the helically corrugated waveguide gyro-TWT has been found in close agreement with the experimentally tested amplifier. It is hoped that the present numerical modelling and benchmarking studies would be helpful to further improve the performance of the gyro-TWT amplifier using helically corrugated waveguide as its RF interaction circuit.